Radiating Shock Measurements in the *Z*-Pinch Dynamic Hohlraum

G. A. Rochau,[1] J. E. Bailey,[1] Y. Maron,[2] G. A. Chandler,[1] G. S. Dunham,[3] D. V. Fisher,[2] V. I. Fisher,[2] R. W. Lemke,[1]
J. J. MacFarlane,[4] K. J. Peterson,[1] D. G. Schroen,[5] S. A. Slutz,[1] and E. Stambulchik[2]

[1]*Sandia National Laboratories, Albuquerque, New Mexico 87185, USA*
[2]*Weizmann Institute, Rehovot, Israel*
[3]*K-tech Corporation, Albuquerque, New Mexico 87185, USA*
[4]*Prism Computational Sciences, Madison, Wisconsin 53704, USA*
[5]*General Atomics, San Diego, California 92186, USA*
(Received 23 October 2007; published 28 March 2008)

The *Z*-pinch dynamic hohlraum is an x-ray source for high energy-density physics studies that is heated by a radiating shock to radiation temperatures >200 eV. The time-dependent $300-400$ eV electron temperature and 15–35 mg/cc density of this shock have been measured for the first time using space-resolved Si tracer spectroscopy. The shock x-ray emission is inferred from these measurements to exceed 50 TW, delivering >180 kJ to the hohlraum.

The *Z*-pinch dynamic hohlraum (ZPDH) has demonstrated the capability to deliver >40 kJ of absorbed x-ray energy to an inertial confinement fusion (ICF) capsule, which is $\approx 1/4$ the energy required for ignition [1–4]. The ZPDH is formed when an annular tungsten (*W*) *Z*-pinch plasma is accelerated onto a low-density CH_2 foam converter. The resulting impact launches a radiating shock that propagates radially inward. Radiation from the shocked converter is trapped by the *W* thereby creating a hohlraum. This Letter reports on x-ray spectroscopy measurements of the shocked plasma temperature (T_e) and density (ρ). Over the 5 ns measured interval, it is concluded that (1) the shock ρ increases from 15 mg/cc to 35 mg/cc and T_e decreases from 400 eV to 300 eV, (2) the shocked plasma x-ray emission delivers >180 kJ to the hohlraum, and (3) present ZPDH simulations predict reasonable shock densities but overpredict the shock pressure.

Radiating shocks are also of general interest in astrophysical plasmas and are observed in high-mass stars, accretion flows around black holes, and supernovae [5,6]. In astrophysical *radiative* shocks [5], the radiation flow is diffusive and the shock Mach number *M* is greater than a critical value M_{rad} above which the compressibility of the medium can exceed the hydrodynamical value of $(\gamma + 1)/(\gamma - 1)$. In the ZPDH considered here, the radiation flow in the CH_2 converter is not completely diffusive and $M/M_{rad} \approx 0.92$. Using a converter material with a higher average atomic number (i.e., SiO_2), the lower resulting M_{rad} and more diffuse radiation flow could make the ZPDH shock directly relevant to astrophysical interests at speeds and emission intensities much higher than previously studied [7].

The ZPDH on Sandia's *Z* facility is a 12-mm-tall nested *Z* pinch consisting of a 40/20 mm diameter outer/inner *W* wire array and a 6 mm diameter ≈ 14 mg/cc CH_2 foam converter centered on the axis (Fig. 1). The conditions of the hohlraum are measured with a variety of diagnostics including x-ray diodes, x-ray pinhole cameras, and spectrometers. These have a view of the source shock through apertures on each end of the hohlraum [3,8].

The existence of the strong radiating shock was first measured with x-ray pinhole camera images (Fig. 1) [9]. These images showed a ring of emission that was circular to $< \pm 4\%$, with a standard deviation in the emission intensity of $< \pm 30\%$ as a function of angle around the ring. The shock trajectory measured from a compilation of similar emission data (typically filtered for $h\nu > 800$ eV) from 29 separate experiments is shown in Fig. 2. The mean emission radius at any given time is determined by taking radial lineouts every 10 deg and averaging the centroid location of the emission peaks. The uncertainty in each point is the standard deviation in the centroid locations and ranges from $\pm 2\%$–8%. The data are time tied between experiments by fitting the measurements from each experiment with a line, and time shifting so that the lines pass through the origin. The mean shock speed is determined to be 32.6 cm/μs with a standard deviation of 2.5 cm/μs.
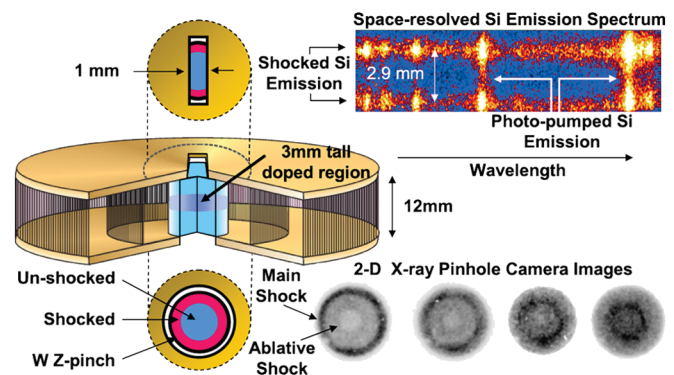

FIG. 1 (color). Dynamic Hohlraum schematic diagram, space-resolved emission spectrum from frame 4 of Fig. 3, and x-ray pinhole images corresponding from left to right to times of -5.7, -5.0, -3.7, and -2.9 ns on the time base of Fig. 2. A 1 mm wide slot aperture is used to provide 1D resolution of the 2D shock for the time- and space-resolved spectral measurements.
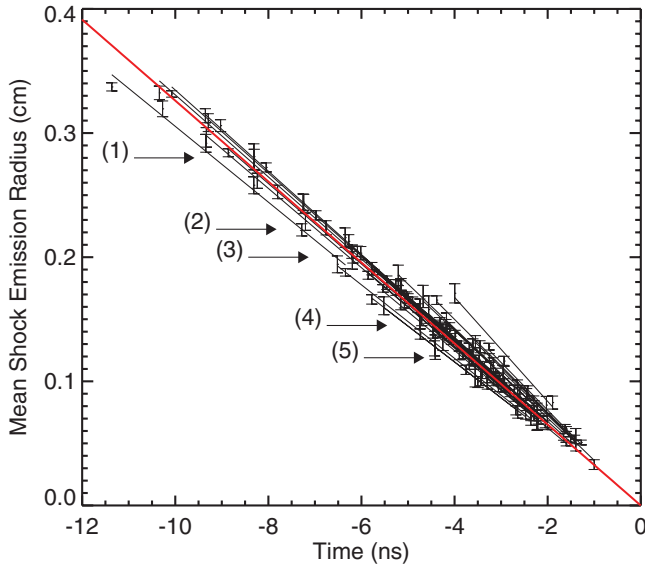
FIG. 2 (color). ZPDH shock trajectories from 29 separate experiments compared to the mean speed of 32.6 cm/μs (red line) on a time base where the peak of the broadband axial power emission occurs at ≈ -2.5 ns. The numbers indicate the mean shock-emission radii from the 5 frames of Si spectral data.

The $< \pm 8\%$ shot-to-shot deviation in the shock speed indicates a high degree of reproducibility in the process that drives the shock.

The shocked plasma conditions were inferred through Si emission spectra obtained by doping the central 3 mm height of the CH_2 foam with 2.5% Si_2O_3 (1% Si by atom). The dopant was confined to the central axial region to prevent the influence of hohlraum end effects. The spectra were measured with a time- and one-dimensionally (1D) space-resolving elliptical crystal spectrometer [10] configured with a magnification of 0.5, 100 μm wide imaging slits, and a microchannel plate (MCP) detector [11] with a gain full-width-at-half-maximum (FWHM) of ≈ 250 ps. A pentaerythritol crystal gave a spectral range of 5.15 Å $\leq \lambda \leq 6.8$ Å with a resolving power of $\lambda/\Delta\lambda \approx$ 800. A 1 mm wide by 7 mm long slot aperture was used to limit the field of view in the unimaged direction of the 1D image. This allowed the instrument to spatially separate the shock emission for radii >0.5 mm with a spatial resolution of ≈ 250 μm. The schematic in Fig. 1 shows the fielding geometry and an example spectral image. The two rows of spectral features correspond to the increase in emission intensity from the two sides of the shocked plasma as viewed through the slot aperture. Spatially separating the shocked plasma emission [12] removes ambiguity in the source of the dopant spectral features observed in previous ZPDH experiments [13].

Figure 3 shows measured spectra taken on two separate experiments at Sandia's Z facility. Frames 1, 3, and 5 are from one experiment, and frames 2 and 4 are from a subsequent experiment with nominally the same configuration. The times of each frame were determined by as-

suming that the peak in the radial distribution of the spectral line emission occurs at the same location as the peak of the continuum emission in the 2D pinhole images (Fig. 2). The spectra are taken by averaging over the ± 250 μm spatial region around the peak of the shocked plasma emission. Detector defects and/or clipping limit the present analysis to one side of the visible emission.

The measured spectra are interpreted using self-consistent atomic kinetics and radiative transfer computations at the Weizmann Institute using a model based on [14]. The CH_2 plasma is treated as a hot (shocked) shell surrounding a colder (unshocked) cylindrical cell. The inner and outer radii of the hot shell are determined by the average FWHM of the radial distributions in the measured spectral line intensities. The radiation field at any location in the plasma must be computed self-consistently with the ionic charge states and level populations, including the influence of radiation from the entire plasma. To account for this, the local radiation field is computed by integrating the radiative transfer equation throughout the plasma with the tungsten emission radiation in the boundary conditions. The non-local thermodynamic equilibrium (LTE) rate equations are solved accounting for spontaneous radiative decay, autoionization, photoionization, electron impact ionization and excitation, photoexcitation, and
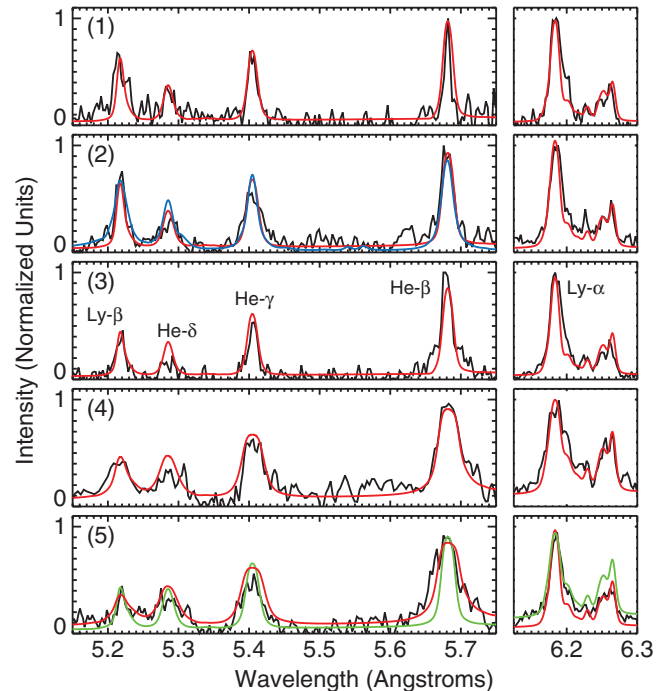

FIG. 3 (color). Measured shocked emission spectra (black lines) compared with spectra calculated by the Weizmann model (red lines) for the best-fit temperature and density conditions at mean shock-emission radii of (1) 2.8 mm, (2) 2.2 mm, (3) 2.0 mm, (4) 1.5 mm, and (5) 1.1 mm. A representative SPECT3D calculation (blue lines) is shown in (2). The green line in (5) shows the Weizmann spectrum that best fits the ratio of the Ly-α to its satellites.

the reverse processes. The spectral line shapes are determined including Doppler and Stark [15] broadening as well as the opacity broadening along each ray in the transport calculations. The observed spectra are simulated assuming the hot shell and central cylinder are each characterized by single (but different) T_e and ρ values, and then computing the radiation emission along the diagnostic line of sight including the integration across the 1 mm wide slot aperture.

The experimental conditions are determined by varying the assumed T_e and ρ until the measured and simulated spectra agree in the widths of each line and in the relative intensities of the Ly-β to the He-β and He-γ, *and* the relative intensity of the Ly-α to its satellites. The simulated shock-emission spectra are insensitive to the conditions in the unshocked plasma for reasonable choices of density (conserving mass) and temperature (100–150 eV in frames 1–3 and 150–250 eV in frames 4–5). A 3% change in the assumed shock T_e produces a greater change in the simulated spectrum than a 70% change in the assumed unshocked T_e or ρ. The simulated spectra at the best-fit shocked T_e and ρ for each time frame (Fig. 4) are overlaid on the data in Fig. 3. The relative intensities of the lines in the simulated spectra have been preserved in the range between the Ly-β and He-β, but the Ly-α and its satellites have been scaled by an independent value to account for uncertainties in the pulsed MCP gain that may affect the relative intensity of lines that are far apart on the MCP stripline. For this reason, the Ly-α is only considered relative to its satellites and not in relation to the other lines in the spectra. The He-δ is not considered in this analysis because calculations indicate its amplitude may be affected by the collectivization of states [16], whereas the present computations use the traditional approximation for continuum lowering [14]. Collectivization may also effect the He-ϵ, which is blended with the Ly-β. If this effect were included, it is estimated to impact the inferred temperature

by ≈ 5 eV due to a decrease in the calculated intensity of the blended Ly-β/He-ϵ feature.

As seen in Fig. 4, the shocked T_e decreases from 400 ± 15 eV to 300 ± 20 eV and the ρ increases from 15 ± 3 mg/cc to 35 ± 7 mg/cc over the ≈ 5 ns spanned by the data. The error bars are determined by visual comparison for small increments in temperature and density, and do not include errors in the spectral model accuracy. An independent analysis of the data was done with the SPECT3D code [17], which includes similar atomic kinetics and radiation transport processes but approximates the Stark broadened line shape as a Voigt with a width determined by fits to MERL calculations [18]. Rather than a visual comparison, each measured and SPECT3D simulated line are fit with a Voigt profile to extract representative intensities and widths. Particular attention is paid to the counting statistics in the measured spectra in order to determine line parameters with uncertainties [19]. The measured line ratios and widths are then compared to those determined from the collection of calculations to determine the best-fit conditions. The error bars are determined from the weighted standard deviation of the line ratios or widths, where the weights are determined from the uncertainties in the line fits. The results of this procedure (Fig. 4) agree with the Weizmann calculations to within the uncertainties. The largest difference between the models is in frame 5. In this frame, the Weizmann model requires a density of ≈ 19 mg/cc to fit the ratio of the Ly-α to its satellites, but a density of ≈ 39 mg/cc to fit the linewidths. This is shown in Fig. 3 and is included in the determination of the uncertainties. The SPECT3D calculations do not properly simulate the very optically thick Ly-α line profile (because of the approximate line shapes) so that the conditions determined with SPECT3D only consider transitions at $\lambda < 6$ Å, which are better fit at higher density. Further measurements are required to determine if the difference in density inferred from the two parts of the spectrum is an instrument effect or requires refinements in the physics model.

The physical processes in the ZPDH are modeled with the LASNEX 2D radiation-magneto-hydrodynamics (RMHD) code [20], which simulates the Z-pinch implosion onto the CH_2 converter and the subsequent formation of the radiating shock [21]. The simulations are constrained by measurements of the shock speed, T_e, and ρ. In general, the simulations predict shock speeds that are $\approx 25\%$–35% higher than the 32.6 cm/μs measurement, shock temperatures that are $\approx 1.5 \times$–$2 \times$ higher than those in Fig. 4, and shock densities that agree to within $\approx 30\%$. These disagreements are caused by a simulated shock pressure that is 15–20 Mbar in comparison to the 5–10 Mbar pressure calculated from the measured T_e and ρ. The elevated simulated shock pressure may be caused by missing or incorrectly modeled physical processes. The LASNEX simulations can not model important 3D effects such as the wire ablation process or azimuthal anticorrela-
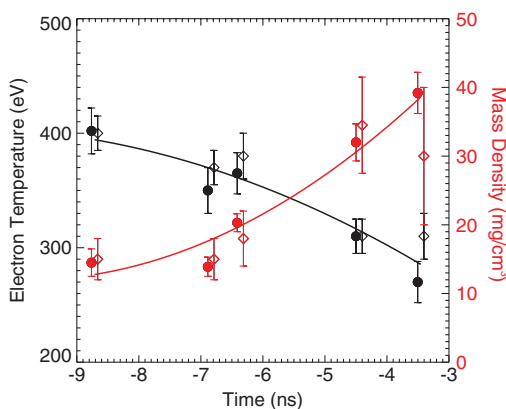

FIG. 4 (color). Best-fit electron temperature (black) and mass density (red) for each spectrum shown in Fig. 3 as calculated by the Weizmann model (diamonds) and SPECT3D (circles). The solid lines are second order polynomial fits to the average of the two models.

tion of instabilities. These effects can change the distribution of mass that impacts the foam and/or lead to current shunting. Work is in progress to incorporate these effects in wire-array Z-pinch simulations [22]. Despite the model limitations, the measured and simulated shock densities are in reasonable agreement. This includes frames 1 and 2, which are nearly unchanged from the original CH_2 foam density. The LASNEX simulations predict that radiation from the early heating and implosion of the W Z-pinch plasma is absorbed near the foam surface, creating an ablative shock that rarefies the CH_2 [21]. The radiating shock is then formed by the collision between the W plasma and rarefied CH_2. Quantitative analysis of the ablative shock that is clearly visible in 2D images (Fig. 1) will be provided in a future publication.

The total x-ray power emitted by the radiating shock is estimated through non-LTE computations of the CH_2 emission from the full 12 mm length of the ZPDH. At the best-fit plasma conditions in frames 1–5, the shock radiates 32 ± 13, 25 ± 10, 27 ± 11, 59 ± 24, and 37 ± 21 TW, respectively, with $\approx 80\%$ of the energy in the interval $100 \text{ eV} \leq h\nu \leq 1000 \text{ eV}$. Integrated over the time of the measurements, the radiating shock delivers ≈ 180 kJ of x-ray energy to the hohlraum. More energy is radiated during the period before the shock reaches the axis. ICF capsules have been demonstrated to absorb >40 kJ of the energy from this shock emission and the reradiation by the W plasma. The emission is calculated to scale as the square of the density but is nearly independent of temperature. From a hohlraum energetics point of view, it is therefore more important for an RMHD simulation to correctly capture the density conditions than the temperature. Thus, LASNEX source power and hohlraum temperature predictions may exceed the actual values by a modest amount, even though the shock temperature is significantly overpredicted.

Finally, the conditions of the plasma ahead of the shock are under investigation. The intense Si-XII and Si-XIII line emission in the shocked plasma radiatively populates the upper states of the corresponding transitions in the unshocked plasma. This "photo-pumping" significantly increases the intensity level of the line emission so that the shocked and unshocked plasma emission are observable on a similar intensity scale. Photopumped line emission from the unshocked plasma is observable on frames 3–5 of the data presented here, and is annotated in the example image of Fig. 1. Plasma conditions inferred from these spectra may be used to determine the conditions ahead of the main shock, including the conditions at the location of an ICF capsule embedded in the foam. This is also important for understanding the influence of radiation on the shock evolution, a critical aspect of radiative shocks in astrophysical plasmas. The ZPDH shock described here differs from that analyzed in [5] because the medium ahead of the shock is optically thin, a situation described in [6]. Making a clear link to radiative shocks in optically thick media will require a converter material with a higher average atomic number. Using a pure SiO_2 converter with $\rho = 50$ mg/cc,

the Rosseland mean optical depth would be >1 across the diameter of the hohlraum for unshocked temperatures <175 eV with $M/M_{rad} > 1$. Such experiments could extend radiative shock measurements to higher shock speed, higher shock emission, and larger spatial scales. Additionally, the lower Z propagation medium would make non-LTE radiative cooling calculations more tractable than the Xe gas often used in laser experiments.

[1] M. K. Matzen *et al.*, Phys. Plasmas **4**, 1519 (1997); V. P. Smirnov, Plasma Phys. Controlled Fusion **33**, 1697 (1991); J. H. Brownel *et al.*, Phys. Plasmas **5**, 2071 (1998).

[2] J. E. Bailey *et al.*, Phys. Rev. Lett. **92**, 085002 (2004); C. L. Ruiz *et al.*, *ibid.* **93**, 015001 (2004); S. A. Slutz *et al.*, Phys. Plasmas **10**, 1875 (2003); J. E. Bailey *et al.*, *ibid.* **13**, 056301 (2006); D. L. Peterson *et al.*, *ibid.* **6**, 2178 (1999); S. A. Slutz *et al.*, *ibid.* **8**, 1673 (2001).

[3] T. J. Nash *et al.*, Phys. Plasmas **6**, 2023 (1999).

[4] J. Lindl, Phys. Plasmas **2**, 3933 (1995).

[5] S. Bouquet, R. Teyssier, and J. P. Chieze, Astrophys. J. Suppl. Ser. **127**, 245 (2000).

[6] R. P. Drake, Astrophys. Space Sci. **298**, 49 (2005).

[7] X. Fleury *et al.*, Laser Part. Beams **20**, 263 (2002); J. C. Bozier *et al.*, Phys. Rev. Lett. **57**, 1304 (1986); J. Grun *et al.*, Phys. Rev. Lett. **66**, 2738 (1991); P. Keiter *et al.*, Phys. Rev. Lett. **89**, 165003 (2002).

[8] T. W. L. Sanford *et al.*, Phys. Plasmas **7**, 4669 (2000); T. J. Nash *et al.*, Rev. Sci. Instrum. **70**, 464 (1999).

[9] J. E. Bailey *et al.*, Phys. Rev. Lett. **89**, 095004 (2002).

[10] P. W. Lake *et al.*, Rev. Sci. Instrum. **75**, 3690 (2004).

[11] G. A. Rochau *et al.*, Rev. Sci. Instrum. **77**, 10E323 (2006).

[12] J. E. Bailey *et al.*, HED Phys. **1**, 21 (2005).

[13] J. P. Apruzese *et al.*, Phys. Plasmas **12**, 012705 (2005).

[14] V. I. Fisher *et al.*, HED Phys. **3**, 283 (2007).

[15] E. Stambulchik and Y. Maron, J. Quant. Spectrosc. Radiat. Transfer **99**, 730 (2006); E. Stambulchik *et al.*, HED Phys. **3**, 272 (2007).

[16] D. V. Fisher and Y. Maron, J. Quant. Spectrosc. Radiat. Transfer **81**, 147 (2003); Eur. Phys. J. D **18**, 93 (2002).

[17] J. J. MacFarlane *et al.*, in *Proceedings of Inertial Fusion Sciences and Applications* (American Nuclear Society, La Grange Park, IL, 2004); J. J. MacFarlane *et al.*, HED Phys. **3**, 21 (2007).

[18] L. A. Woltz and C. F. Hooper, Jr., Phys. Rev. A **38**, 4766 (1988); R. C. Mancini *et al.*, Comput. Phys. Commun. **63**, 314 (1991).

[19] G. S. Dunham *et al.*, Rev. Sci. Instrum. **78**, 063106 (2007).

[20] G. B. Zimmerman and W. L. Kruer, Comments Plasma Phys. Control. Fusion **2**, 51 (1975).

[21] R. W. Lemke *et al.*, Phys. Plasmas **12**, 012703 (2005); S. A. Slutz *et al.*, *ibid.* **13**, 102701 (2006).

[22] E. P. Yu *et al.*, Bull. Am. Phys. Soc. **52**, 98 (2007).